Podosomes Display Actin Turnover and Dynamic Self-Organization in Osteoclasts Expressing Actin-Green Fluorescent Protein⩔

Olivier Destaing,*† Frédéric Saltel,*† Jean-Christophe Géminard,‡ Pierre Jurdic, and Frédéric Bard*§‖

*Laboratoire de Biologie Moléculaire et Cellulaire, Unité Mixte Recherche 5665, Centre National de la Recherche Scientifique/ENS, INRA 913, Lyon, France; and ‡Laboratoire de Physique, Unité Mixte Recherche 5672, Centre National de la Recherche Scientifique-ENS Lyon Ecole Normale Supérieure de Lyon 46, allée d'Italie, 69007 Lyon, France

Podosomes, small actin-based adhesion structures, differ from focal adhesions in two aspects: their core structure and their ability to organize into large patterns in osteoclasts. To address the mechanisms underlying these features, we imaged live preosteoclasts expressing green fluorescent protein-actin during their differentiation. We observe that podosomes always form inside or close to podosome groups, which are surrounded by an actin cloud. Fluorescence recovery after photobleaching shows that actin turns over in individual podosomes in contrast to cortactin, suggesting a continuous actin polymerization in the podosome core. The observation of podosome assemblies during osteoclast differentiation reveals that they evolve from simple clusters into rings that expand by the continuous formation of new podosomes at their outer ridge and inhibition of podosome formation inside the rings. This self-organization of podosomes into dynamic rings is the mechanism that drives podosomes at the periphery of the cell in large circular patterns. We also show that an additional step of differentiation, requiring microtubule integrity, stabilizes the podosome circles at the cell periphery to form the characteristic podosome belt pattern of mature osteoclasts. These results therefore provide a mechanism for the patterning of podosomes in osteoclasts and reveal a turnover of actin inside the podosome.

INTRODUCTION

Podosomes are adhesion structures found in osteoclasts, macrophages, and Rous sarcoma-transformed cells (Marchisio *et al.*, 1984, 1987; Tarone *et al.*, 1985; Nermut *et al.*, 1991). They share with focal adhesions several proteins such as integrins (Zambonin Zallone *et al.*, 1989; Helfrich *et al.*, 1996; Nakamura *et al.*, 1999), vinculin, paxillin, and talin (Marchisio *et al.*, 1988; DeFife *et al.*, 1999). However, podosomes clearly differ from focal adhesions or focal complexes in the structural organization of these various proteins. Instead of a cluster of integrins linked to actin stress fibers by a large multimolecular adaptor formed of structural and signaling proteins, podosomes are formed of a diffuse membrane domain of integrins and associated proteins surrounding a dense actin core (Pfaff and Jurdic, 2001). The mechanisms that regulate this structure are not known at present but probably involve the actin regulators that are specifically found in podosomes and not focal adhesions, like cortactin and Wiskott-Aldrich syndrome protein (WASP), which localize directly underneath the podosome (Pfaff and Jurdic, 2001), and gelsolin, an actin-severing agent essential for podosome regulation (Gavazzi *et al.*, 1989; Chellaiah *et al.*, 2000).

Although podosomes are present in other cell types, it is only in mature osteoclasts that they arrange into a precisely defined circle at the cell periphery. Osteoclasts are giant multinucleated bone-resorbing cells formed by fusion of monocytic precursors after stimulation by receptor activator of nuclear factor B-ligand (RANK-L) and macrophage colony-stimulating factor (M-CSF) (Burgess *et al.*, 1999; Shevde *et al.*, 2000). The podosome belt found in mature osteoclasts is

thought to evolve into the sealing zone in actively resorbing osteoclasts (Lakkakorpi *et al.*, 1989), forming a large circular band of actin that provides tight attachment to the bone and seals off the resorption pit where proteases and protons are secreted (Vaananen *et al.*, 2000).

The mechanism by which podosomes can arrange at such a large scale is not known at present. The microtubule network, which is also organized at the scale of the whole cell, is thought to be self-organized as defined by Gerhart and Kirschner (1997). The patterns formed can then be selected and eventually stabilized by external mechanisms, allowing a great flexibility and adaptability, as exemplified by the various organizations of microtubule networks in different cell types. Interestingly, microtubules have been reported to regulate the distribution of podosomes in osteoclasts (Babb *et al.*, 1997) and possibly their formation in macrophages (Linder *et al.*, 2000).

To address podosome dynamics and podosome pattern formation, we have generated a monocytic cell line expressing an actin-green fluorescent protein (GFP). This cell line can be induced to differentiate into osteoclasts using RANK-L and M-CSF. Using live confocal imaging, we probed individual podosomes by fluorescent recovery after photobleaching (FRAP) analysis and compared the dynamics of actin and cortactin. Our results indicate that actin turns over in the podosome core. We found also that podosomes form a dynamic assembly, the expanding ring, which explains how they can be restricted at the cell periphery in mature osteoclasts. Finally, we show that microtubules play an essential function in the stabilization of rings at the cell periphery.

MATERIALS AND METHODS

Reagents

pEGFP-Actin Vector was from BD Biosciences Clontech (Palo Alto, CA). PDsRed-N1 cortactin is a gift from Marko Kaksonen (University of Helsinki, Helsinki, Finland). Nocodazole (Sigma-Aldrich, St. Louis, MO) was used at 2 μM. A yeast culture supernatant containing recombinant human RANK-L was produced from *Pichia* yeast, a kind gift from Nordic Biosciences (Copenhagen, Denmark). Supernatant of methanol-induced yeast was dialyzed against α-minimal essential medium (α-MEM) and used at a final dilution of 3%, equivalent to ~20 ng/ml recombinant soluble RANK-L (R & D Systems, Minneapolis, MN). Human M-CSF was produced in culture medium of COS cells transfected as described previously (Bourette *et al.*, 1993). Supernatant was used at a final dilution of 1% corresponding to ~20 ng/ml recombinant M-CSF (R & D Systems). Anti-vinculin (clone Vin11-5), monoclonal antibody AC40, anti-actin, and anti-acetylated tubulin monoclonal antibody 6-11B-1 from were from Sigma-Aldrich; anti-β tubulin (clone N357) was from Amersham Biosciences (Piscataway, NJ); and anti-paxillin (clone 349) was from Transduction Laboratories (Lexington, KY). F-actin distribution was revealed after incubation with tetramethylrhodamine B isothiocyanate-conjugated phalloidin (Molecular Probes, Eugene, OR). Coverslips were mounted in Prolong antifade (Molecular Probes). Telomeric repeat amplification protocol (TRAP) activity was revealed by acid phosphatase, leukocyte kit (Sigma-Aldrich) according to manufacturer's recommendations.

Osteoclast Differentiation

Spleen cells of 6–8-wk-old male mice OF1 were seeded at 2500 cells/mm² and were cultured for 8 d on coverslips in differentiation medium: α-MEM (Invitrogen, Carlsbad, CA) medium containing

10% of fetal calf serum (Hyclone Laboratories, Perbio Science, Cheshire, United Kingdom), 20 ng/ml M-CSF, and 20 ng/ml soluble recombinant RANK-L. RAW 264.7 cells were from American Type Culture Collection (Manassas, VA) and transfected with Fu-GENE 6 following manufacturer's recommendations (Roche Diagnostics, Indianapolis, IN). The stable actin-GFP RAW cell line was seeded at a density of 100 cells/mm² in differentiation medium to induce osteoclastogenesis.

Resorption Test

Actin-GFP RAW cells were seeded on dentine slices (a generous gift from Drs. Suda and Takakhoshi, Matsumoto Dental University, Nagano, Japan) and incubated in differentiation medium for 12 d. To visualize resorption pits, dentine slices were first scraped out in water containing 1% Triton X-100 to eliminate cells and stained with toluidine blue (Arnett and Dempster, 1987).

Microinjection

Mouse spleen cell-derived osteoclasts differentiated in vitro on Eppendorf CELLocate coverslips for 7 d in differentiation medium were transferred into observation medium. Intranuclear microinjection of actin-GFP cDNA (0.2 mg/ml in 0.05 M Tris-HCl pH 7.4) was performed at room temperature on an Eclipse TE 200 inverted microscope (Nikon, Tokyo, Japan) by using a micromanipulator InjectMan and a microinjector 5246 from Eppendorf (Hamburg, Germany). After injection, cells were further maintained at 37°C and 5% CO_2 for 6 h in differentiation medium before imaging.

Time-Lapse and Confocal Microscopy

Osteoclasts were differentiated in 35-mm glass-bottom Petri dishes then transferred at 37°C into observation medium: α-MEM without bicarbonate (reference 11900; Invitrogen) containing 10% of fetal calf serum, 20 ng/ml M-CSF, 20 mM HEPES, and 20 ng/ml soluble recombinant RANK-L. The dishes were placed on a 37°C heated stage (Carl Zeiss, Jena, Germany), and cells were imaged with a laser scanning microscope 510 (Axiovert 100 M) and a 40× (numerical aperture 1.0) Plan-Apochromat objective (all from Carl Zeiss). Meta Imaging Series 4.5 (Universal Imaging, West Chester, PA) was used to mount AVI movies from image stacks. Images extracted from stacks were processed with Adobe Photoshop 6.0 (Adobe Systems, San Jose, CA). FRAP experiments were carried out at 488 nm and at maximum power for two iterations (2.8-s bleach) and quantification was made with LSM 510 software (Carl Zeiss). For immunofluorescence, cells were fixed in 3.7% formaldehyde, processed as described previously (Ory *et al.,* 2000), and imaged with an LSM 510 (Carl Zeiss) by using a 63× (numerical aperture 1.4) Plan Neo Fluor objective. To prevent cross-contamination between fluorochromes, each channel was imaged sequentially using the multitrack recording module before merging.

FRAP Quantification

Image analysis was performed with Scion Image (Scion, Frederick, MD) on PC. For actin-GFP, the life span of the podosomes being not much larger than the FRAP characteristic time, the fluorescence recovery had to be measured specifically within podosomes that existed during the whole recovery time. The regions corresponding to these podosomes were located by the combination of two masks. The masks [M1] and [M2] correspond to the brightest points (i.e., the podosomes) before and after photobleaching, respectively. Applying the masks [M1] and [M2] to the images made it possible to measure the intensity of the fluorescent light within the podosomes that existed during the whole recovery time. In contrast, excluding the points belonging to the masks [M1] and [M2] from the images made it possible to measure the fluorescent light within the cloud, excluding all the podosomes. The interpolation of the experimental data by an exponential law (performed with Igor Pro 4.0; Wave-
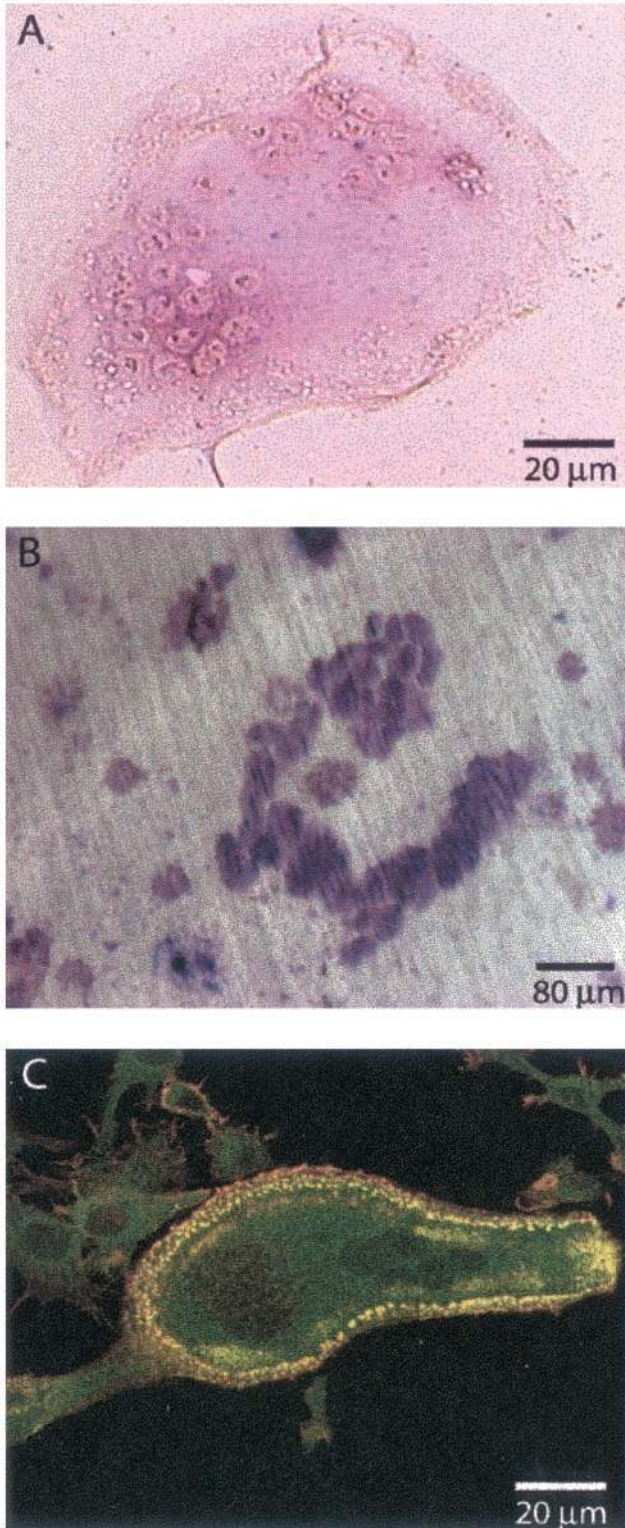
Metrics, Lake Oswego, OR) on PC gave the characteristic times of fluorescence recovery within the podosomes and within the cloud. For cortactin-RFP, the FRAP was measured in the area of photobleaching.

RESULTS

A RAW Cell Line Stably Expressing Actin-GFP Can Differentiate into Osteoclasts

The murine macrophage RAW cell line can differentiate into osteoclasts in the presence of RANK-L (Shevde *et al.*, 2000). To study the dynamics of the actin structures in osteoclasts, we generated a RAW cell clone stably expressing an actin-GFP chimera. This cell line differentiated into functional osteoclasts upon exposure to RANK-L and M-CSF, with similar kinetics to primary mouse splenocytes, i.e., in ~8 d, as verified by TRAP staining, a marker for osteoclasts (Figure 1A); and by the ability to resorb bone (Figure 1B). Actin-GFP colocalized with rhodamine-phalloidin in these cells (Figure 1C) at all stages of differentiation, indicating that actin-GFP functions as the endogenous actin, as was reported previously (Ballestrem *et al.*, 1998; Choidas *et al.*, 1998). The RAW actin-GFP–derived osteoclasts seemed, therefore, very similar to osteoclasts derived either from primary spleen cells or from the parental RAW cell line. Nevertheless, we verified that dynamic events in RAW-derived osteoclasts were not cell line dependent by micro-injecting primary osteoclasts with the actin-GFP expression vector (see, for example, Movie 3). In these cells, we observed that podosomes had a similar life span and were able to form the three different types of pattern described herein for RAW-derived osteoclasts.

Podosomes Are Clustered Inside "Clouds" of Actin-GFP in Premature Osteoclasts

At early stages of differentiation, podosomes in osteoclasts were grouped in several clusters of various size and shape. In negative images, podosomes looked like dark spots of ~0.3-μm apparent diameter, surrounded by a gray actin cloud (Figure 2A). Cell labeling with phalloidin suggests that this actin cloud is formed at least in part of actin filaments (our unpublished data). In three-dimensional reconstitution, podosomes looked like cones of ~0.5-μm height and the cloud like a thin meshwork adjacent to the membrane (Movie 1). Typical focal adhesion proteins such as paxillin and vinculin colocalize with the cloud (Pfaff and Jurdic, 2001; our unpublished data), whereas actin regulatory proteins such as cortactin (Pfaff and Jurdic, 2001) and gelsolin (Akisaka *et al.*, 2001) colocalize with the podosome core. Podosomes were regularly spaced with in average 1.4 μm between adjacent podosomes. At the border of the clus-

Figure 1. Actin-GFP–expressing RAW cells differentiate into osteoclasts. Actin-GFP RAW cells were stimulated daily with RANK-L/M-CSF to induce differentiation. (A) After 8 d, fully differentiated, multinucleated osteoclasts are revealed by TRAP activity (purple stain). (B) Resorption pits (dark purple) formed after 12 d of culture on dentine slices. (C) A single osteoclast is shown with a podosome belt; colocalization of actin-GFP (green) with phalloidin-rhodamine-isothiocyanate (red) is revealed by yellow/orange color.
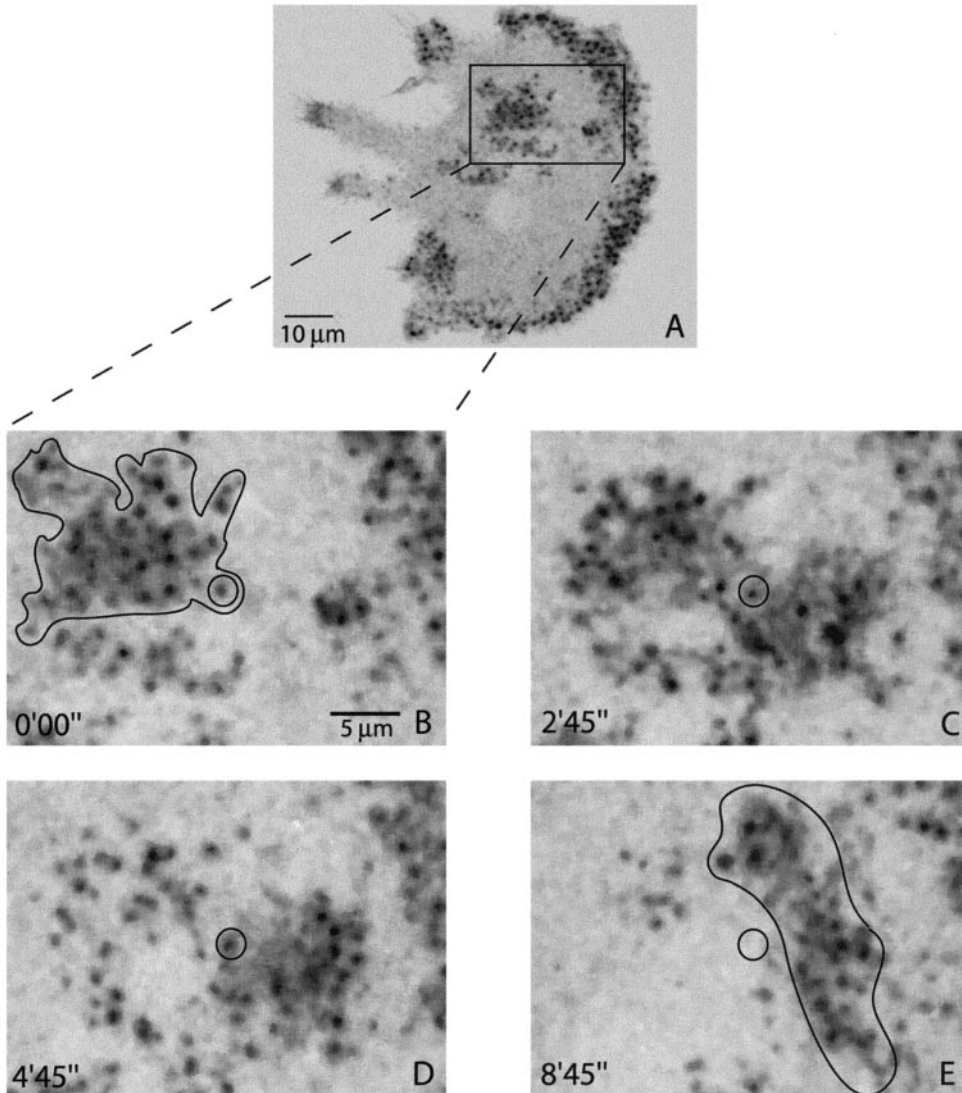
Figure 2. Podosome clusters move with a play of podosome assembly and disassembly. A murine primary osteoclast intranuclearly microinjected with an actin-GFP expression plasmid was observed by confocal time-lapse microscopy. GFP fluorescence images were inverted for better visualization and significant frames were extracted. (A) Overview of the cell that shows the different clusters. (B–E) Zoom on a cluster delineated by a dark line and composed of podosomes (black dots) surrounded by an actin cloud (gray). Although the whole structure (delimited by the dark line in B and E) has completely translated in 9 min, specific podosomes did not move as exemplified by the circled podosome.

ter, the cloud of actin-GFP was centered on each podosome and extended ~1 μm from the edge of each podosome. Within the cluster, the cloud looked like a continuum between surrounding podosomes (Figure 2, B–E). During time-lapse observations, the clusters were stable for up to several hours (Movie 2), whereas the median podosome life span was 2 min (Table 1). Podosome clusters were very variable in shape and size, but they kept their cohesion while moving and could be tracked over time as exemplified in Figure 2 (black over line in Figure 2, B and E). In contrast, podosomes inside the cluster did not move (Figure 2, B–D, circle). Movement of the clusters involved in fact the formation of new podosome at the front and the disassembly of old ones at the rear of the cluster, reminiscent of a caterpillar movement. To better understand the complex structure of the cluster, we then sought to probe actin dynamics inside it.

Table 1. Podosomes have similar life span in clusters, rings, and belts

|	Clusters	Rings	Belts
Median life span of podosomes	2 min 16 sec	2 min 20 sec	2 min
Average life span	2 min 33 sec	1 min 50 sec	2 min 53 sec
Standard deviation	± 1 min 31 sec	± 59 sec	±1 min 28 sec
Minimum life span	30 sec	30 sec	1 min
Maximum life span	14 min	3 min 20 sec	10 min 40 sec
No. of cells measured	12	9	14
Speed of expansion	n.d.	2.02 μm sec^{-1} ± 0.83 (n = 18)	n.d.

n.d., not determined.

Figure 3. FRAP analysis indicates actin turnover in podosomes. Osteoclasts derived from actin-GFP and cortactin-RFP RAW cells were imaged using fluorescein-type and rhodamine-type filter set, respectively. Actin and cortactin (A and A′), respectively, before photobleaching; after photobleaching in the white box (B and B′); and first image showing complete recovery of photobleaching (C and C′). (D and D′) Overlay of A, B, and C (A′, B′, and C′, respectively) white dots result from podosomes present in all three images; yellow signals podosomes present in A and C (A′ and C′, respectively). The lack of "yellow" podosomes in D′ compared with D illustrates that cortactin does not turnover in individual podosomes, whereas actin does. (E) Actin-GFP fluorescence over time in podosomes and in the cloud quantified using masks (see MATERIALS AND METHODS) after photobleaching. Both experimental data sets fit an exponential law with a similar characteristic time of 30 s (dashed lines). (E′) Cortactin-RFP fluorescence recovery measured in the whole area photobleached, the data set fits an exponential law (dashed line) with a characteristic time of 3 min. Experiment representative from five independent measures. (F) Plot of the characteristic time of FRAP in podosome (τ_{podo}) vs. the characteristic time of the cloud (τ_{cloud}) in 11 independent experiments. Although the characteristic time varies from 20 to 45 s, τ_{cloud} and τ_{podo} remain tightly correlated. Bar, 5 μm.
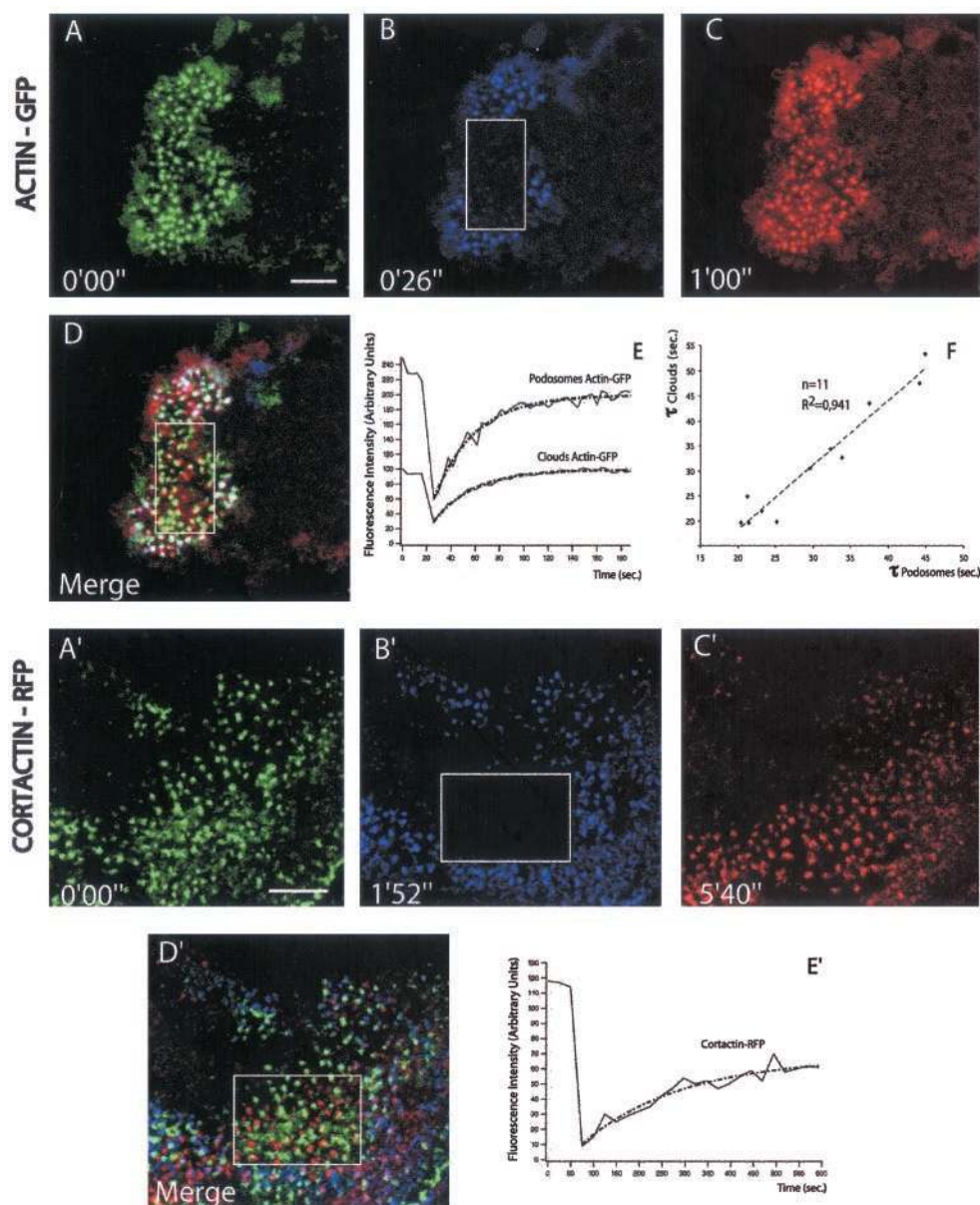
FRAP Analysis Reveals Actin Turnover in Podosomes and Shows a Correlation between Dynamics of Podosomes and Cloud

To probe the dynamics of actin in podosome arrays, we used a FRAP approach. GFP-actin fluorescence recovered completely in ~1 min in the photobleached area (Figure 3, A–C, and Movie 3). Surprisingly, individual podosomes recovered their fluorescence, indicating that recovery was not due to the assembly of new podosomes but to a high turnover of actin in the podosomes themselves (Figure 3D). To test whether this turnover was specific for actin, we generated cortactin-red fluorescent protein (RFP) RAW-derived osteoclasts and repeated the FRAP experiments with these cells (Movie 3). In contrast to actin-GFP,

individual podosomes did not recover cortactin-RFP fluorescence. In the area photobleached, the fluorescence of cortactin-RFP was recovered in podosomes formed after the bleach (Figure 3, A′–D′). The recovery of cortactin-RFP fluorescence fitted an exponential law (Figure 3E′) with a characteristic time of 3 min directly related to podosomes average life span. Therefore, the high turnover of actin in the podosomes is not due to a remodeling of the whole structure but specifically of the actin filaments. Because latrunculin B treatment abolishes very rapidly the podosome (Movie 3), it is likely that polymerization of new monomers is required for this turnover. Based on the analysis of the FRAP data, we discuss in a section of the supplementary material (Podosome Theo-
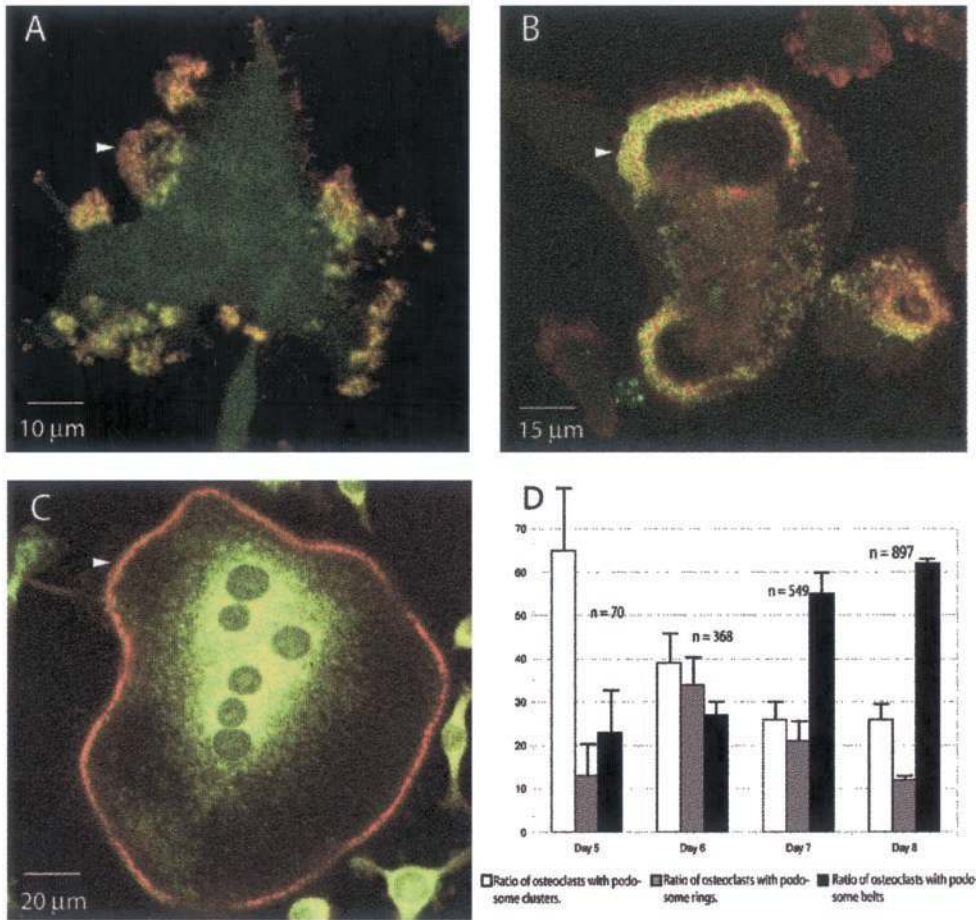
Figure 4. Podosomes are organized after three distinct patterns during osteoclast differentiation. Mouse spleen cells seeded on glass coverslips were induced into osteoclast differentiation with RANK-L and M-CSF for up to 8 d, fixed every day, and double stained for actin with phalloidin-rhodamine-isothiocyanate (red) and for vinculin (green). The first osteoclasts ($\geq$3 nuclei/cells) with podosomes were visible at day 5. A single osteoclast is shown in each picture, podosomes look like red dots circled with green. They are grouped (arrowhead) either in clusters (A), rings (B), or belts (C). The ratio of cells displaying these structures to the total number of osteoclasts counted for each day (n) is shown in D. Rings appeared as a transient structure during the differentiation process.

retical Description) what mechanism could explain the removal of actin.

To measure and compare the kinetics of fluorescence recovery specifically in the podosomes and in the cloud, we developed a signal analysis method based on masks (see MATERIALS AND METHODS). This method measured the variation of fluorescence in all the podosome cores present before the bleach and after complete recovery in a specific area. The fluorescence recovery in the podosome cores fitted closely an exponential law (Figure 3E) with a characteristic dynamical time, $\tau_{\text{podosomes}}$, ranging from 20 to 40 s, depending on the cell considered (Figure 3F). Therefore, during the usual 2-min life span of podosomes, ~2.5 times the amount of actin that composes a podosome at a given time is incorporated and removed from it. Another combination of masks was used to measure fluorescence in the cloud and, interestingly, τ_{cloud} was very close to $\tau_{\text{podosomes}}$. In different experiments, the values of $\tau_{\text{podosomes}}$ and τ_{cloud} were directly proportional (Figure 3F), suggesting a direct link between the two pools of actin.

Three Types of Podosome Organizations Are Found during Osteoclast Differentiation

In premature osteoclasts, podosomes were clustered in patches distributed over the ventral surface of the cell (Fig-

ures 2C and 4A). However, this pattern evolves during differentiation as reported previously (Burgess *et al.*, 1999) and, in mature multinucleated osteoclasts, podosomes accumulate at the cell margin on a narrow circular band, referred to as the belt (Figure 4C). To study the transition between these two patterns, we induced mouse splenocytes with RANK-L and M-CSF to differentiate into multinucleated, fully mature osteoclasts and double stained them at each day of differentiation for actin and vinculin. Podosomes were therefore unambiguously identified as actin-dense dots surrounded by vinculin. The formation of multinucleated osteoclasts with a belt took ~8 d under these conditions. At day 5, ~65% of the cells displayed their podosomes in clusters, whereas by day 8, they were only 25% (Figure 4D). In contrast, cells displaying a belt increased from only 20% at day 5 to ~60% at day 8 (Figure 4F). Interestingly, at day 6 and 7 of differentiation, we observed podosomes in intermediate circular structures different from the belts. These structures, which we coined podosome rings, seemed randomly localized inside the cell in contrast with the peripheral belt (Figure 4B). Furthermore, if a single cell contains several rings or a mix of rings and clusters, the belt is the only podosome array inside a cell. Multinucleated cells containing rings reached a maximum of ~30% at day 6 and their proportion decreased to 12% by day 8 (Figure 4E), indicating
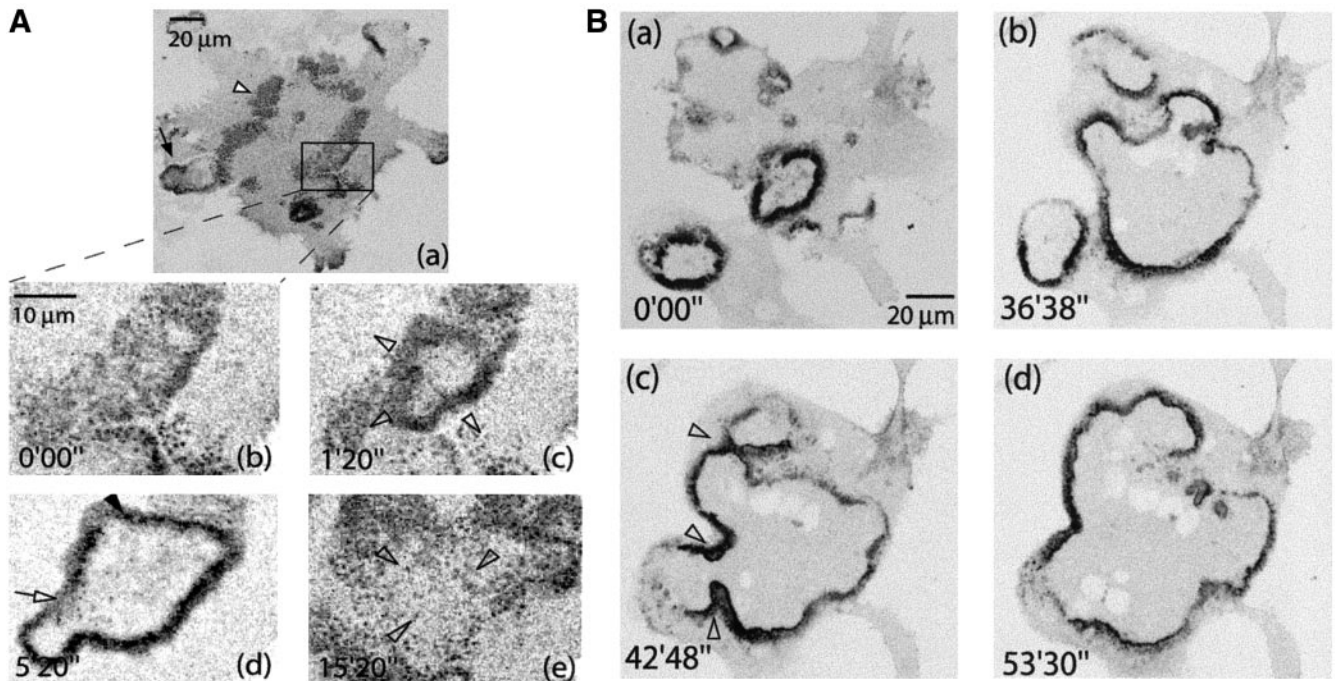
Figure 5. Expanding podosome rings are formed inside podosome clusters and grow larger as differentiation progresses. (A) Actin-GFP RAW osteoclasts at early stage of ring formation (a) overview of the cell with a mix of rings (black arrow) and clusters (white arrowhead). (b–e) Zoomed area. Inside a cluster (b), a ring formed and expanded (c). No podosome formation was observed inside the area delimited by the ring. (d) The ring eventually stopped and collapsed back to a cluster. (B) Osteoclast at later stage of ring formation. Three different rings formed asynchronously from different areas of the cell (a); thus, rings expanded (b) and eventually fused (c). Resultant ring progressed to the periphery (d).

that rings correspond to a transient podosome organization in the course of osteoclast differentiation. Similar results were obtained using the RAW cell line induced into differentiation; therefore, we sought to study podosomes rings by using dynamic imaging in this system.

Rapidly Expanding Podosome Rings Evolve from Podosome Clusters

To study the transition from podosome clusters to rings, actin-GFP–expressing RAW cells stimulated with RANL-L and M-CSF were observed by confocal time-lapse microscopy after 4–6 d of stimulation with RANK-L and M-CSF. The first rings were observed at the 5th day of differentiation. They seemed highly dynamic, always in expansion. At early stages of maturation, rings initiated inside podosome clusters (Figure 5A and Movie 4). The rings were formed of podosomes and a dense cloud. As in the clusters, podosomes per se did not move; the expansion of the ring was rather an outward wave of podosome formation (Movie 4). The life span of podosomes in this structure was very similar to their life span in clusters (Table 1). Also, like in the clusters, the podosomes per se were not moving. The speed of expansion of the ring was of ~2 μm min^{-1} and relatively constant between osteoclasts ($\pm$0.83 μm min^{-1}, n = 18; Table 1). Inside the ring, no podosomes were formed and the rings induced the disappearance of clusters as they progressed through them (Figure 5A, c–e). At early stages, rings

lasted only a few minutes (Figure 5A, d and e) and they remained small compared with the cell size. As differentiation progressed, they lasted up to 1 h and expanded over a broad surface (Figure 5B and Movie 5). At late stages they collapsed, usually only when they reached the edges of the cell (Movie 5). At these stages, rings were formed at a high frequency and the clusters became very transient. Strikingly, rings displayed the ability to fuse with each other (Figure 5B, b and c) to form a larger ring. The fusion refers to the fact that the two waves of podosome assembly coming face to face, instead of progressing "through" each other, were rather reorganized into one wave progressing toward the periphery of the cell. This wave progressed faster than in other parts of the ring, which seemed unaffected by the fusion, allowing for a quick resorption of the "neck" (Figure 5B, e–f, and Movie 5).

Podosomes Belt Is a Stable Structure at Periphery of Cell

After 1 to 2 days of ring formation, extension, and dissociation, a ring eventually stabilized at the cell periphery, and at day 8 of differentiation, >60% of primary osteoclasts displayed a circular row of podosomes at their periphery (Figure 4, C and F). Although the shape of this structure is reminiscent of the ring described previously, belts were, contrary to the rings, stable for several hours, with a limited displacement of the podosome row (Movie 6). Nevertheless,
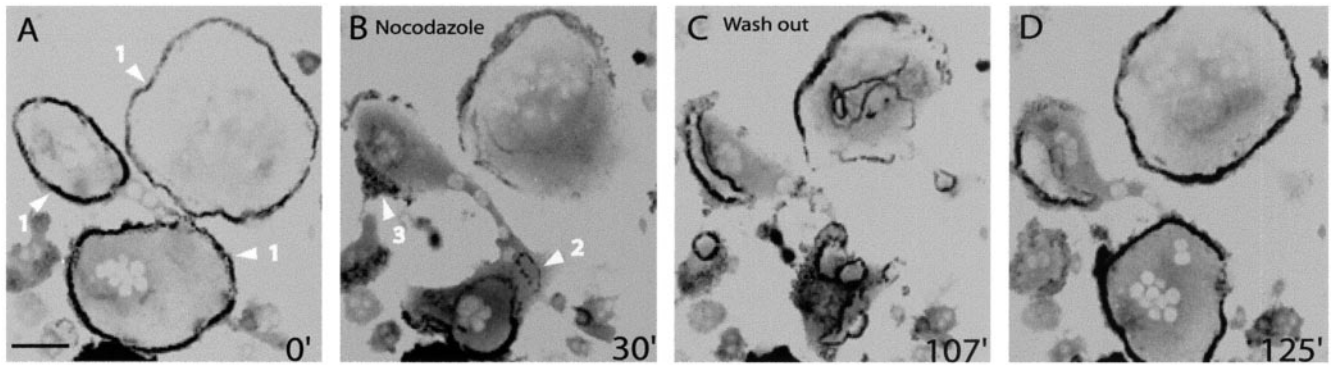
Figure 6. The belt is rapidly destabilized by a nocodazole treatment and is reformed after washout. Actin-GFP RAW osteoclasts at late stages of maturation were imaged by time-lapse confocal fluorescence microscopy. (A) Podosome belts in two different cells (arrowheads 1) were stable before the treatment. (B) After 30 min of a 2 μM nocodazole treatment, the belts have disappeared and replaced by podosomes rings and clusters (arrowheads 2 and 3). (C) After nocodazole washout more rings were formed and they were more stable. (D) After fusion and stabilization at the periphery, rings reformed two belts. Bar, 50 μm.

this structure was still highly dynamic and the podosome lifetime was similar to the ones in clusters or rings (Table 1).

Transition from Rings to Belt Is Microtubule Dependent

To better characterize this podosome dynamic, we turned to microtubules stability. Indeed, microtubules have been implicated in the control of podosome formation (Linder *et al.*, 2000) and of podosome pattern in osteoclasts (Babb *et al.*,

1997). At early stages of osteoclast differentiation, microtubules depolymerization by nocodazole treatment had no visible effect on podosomes clusters and rings (Movie 7). However, at late stages of differentiation, microtubule depolymerization induced a drastic disorganization of the podosome belt (Figure 6 and Movie 7B). Starting as early as 5 min after addition of nocodazole, the podosome belt retracted inwardly and collapsed (Figure 6A, arrowheads 1). By 30 min of treatment, the belt had been replaced by several rings
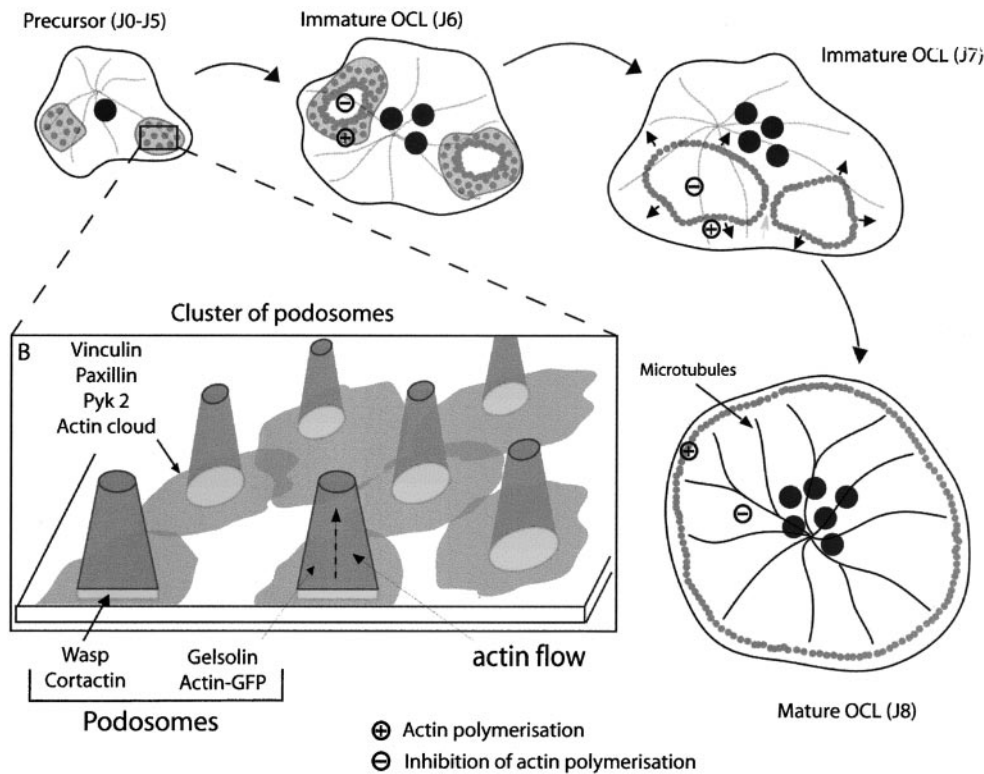
Figure 7. Models of podosome internal dynamics and podosome self-patterning. The integrins and associated proteins such as vinculin and paxillin surround the actin core and presumably induce the formation of a patch of cortactin/WASP-Arp2/3 that controls the actin polymerization. The actin core of the podosome is produced by the combined action of actin polymerization and actin severing. During osteoclastogenesis, rings start to from inside clusters and expand. The ring dynamics constantly induce the formation of new podosomes at its outer ridge while inhibiting new podosomes to form inside. This mechanism drives progressively the formation of podosomes at the cell periphery. A functional microtubule network is needed to stabilize the podosome belt at the cell periphery.

and clusters (Figure 6B, arrowheads 2 and 3), which seem in contrast to the belts, not sensitive to microtubule depolymerization. After nocodazole washout, rings extended toward the periphery (Figure 6C), fused, and finally stabilized as they reached the periphery (Figure 6D). Hence, the microtubules seem to promote dynamically the stabilization of the podosome belt at the cell periphery but are not required for the formation of podosomes rings and clusters.

DISCUSSION

Podosomes are found in cells transformed by v-src (Tarone *et al.*, 1985) and in macrophages and osteoclasts. In osteoclasts, they present the unique ability for adhesion structures to organize in large circular arrays. Podosomes present also a peculiar structure with an actin core that forms a column of 0.3 μm in diameter and ~0.6 μm in height (Marchisio *et al.*, 1988; Nermut *et al.*, 1991) surrounded by a membrane domain enriched in integrins and adaptor proteins such as, for example, vinculin and paxillin (Marchisio *et al.*, 1984, 1987).

Our imaging of actin-GFP podosomes indicates that podosomes are also surrounded by an actin cloud. A FRAP analysis of podosomes and the surrounding cloud indicates that the two structures are dynamically correlated. Furthermore, FRAP shows that the turnover of actin in the core is 2 to 3 times faster than the podosome turnover itself or the turnover of cortactin-RFP. This suggests that the actin cloud could derive from the podosome core. Although the mechanism by which actin turns over in the core is not known at present, some elements suggest what could be its main principles. For actin addition, the rapidly destabilizing effect of latrunculin B over podosomes indicates that actin monomers are required and polymerization likely. This is consistent with the presence of a complex of protein regulating actin polymerization composed of cdc42, WASP, and the Arp2/3 complex (Linder *et al.*, 1999, 2000). In lamellipodia, this complex has been shown to function at the membrane and our own confocal analysis indicates that these proteins are localized at the base of the podosome (Pfaff and Jurdic, 2001), suggesting that polymerization occurs from the basal plasma membrane. Interestingly, this could explain an early observation by electronic microscopy (Gavazzi *et al.*, 1989) and interference reflection microscopy (Tarone *et al.*, 1985) that the actin core of the podosome protrudes on the ventral surface of the cell. By analogy with the lamellipodia, polymerization could induce a force pushing the membrane downwards. For actin removal, it could conceivably occur either at the tip of the podosome or be distributed over the whole height. In the first case, the shape of the FRAP curve should be linear until it reaches a plateau, whereas in the second case, the curve would be exponential as it is in our experimental measures. Then, two types of mechanisms could possibly limit the growth of polymerizing filaments and be distributed over the whole length of the filaments: a depolymerization occurring randomly after the beginning of polymerization or a severing occurring also randomly over the length of the growing filament. The second mechanism seems more likely for two reasons. It is consistent with the concentration of gelsolin, an actin-severing enzyme (Wegner *et al.*, 1994), in the podosome (Gavazzi *et al.*, 1989; Akisaka *et al.*, 2001; our unpublished observation). It is also consistent with our observation of the actin cloud radiating from podosome cores and being dy-

namically correlated to the actin core. This cloud can be labeled by phalloidin and therefore must consist at least in part of polymerized actin. We provide in the supplementary material (Podosome Theoretical Model) a model of a virtual podosome that is regulated only by polymerization at its base and a random severing activity over its whole length. Interestingly, this model shows that these two mechanisms are sufficient to regulate the shape and size of the podosome. Of course, the regulation of a real podosome is likely to be more complex, with microfilaments bundling, capping, and annealing activities all potentially playing a role.

Live imaging of actin-GFP podosomes revealed also that the adhesion structures do not form independently of each other but inside groups. This observation is essential to explain the podosome patterns found in osteoclasts. Indeed, podosomes in mature osteoclasts form a continuous, 2- to 3-μm-wide belt of podosomes at the periphery of the cell that can be 100 μm in diameter and has, roughly, a circular shape. Such a precise distribution is a remarkable achievement, because the cell does not dispose of any external template, as exemplified by the variety of size and shape of these structures, and it must rely on internal mechanisms to produce this large-scale pattern. Interestingly, the modalities of podosome coordination evolve during the differentiation of the osteoclast. At early stages, podosomes are formed inside clusters. At later stages, the podosomes are formed in rings that expand by the continuous assembly of new podosomes at their outer ridge and the disassembly and inhibition of formation on their inner ride (Figure 7). The rings form inside previously existing clusters, suggesting that a maturation of podosome assemblies occurs. A remarkable feature of the rings is their ability to fuse with each other to form larger rings, indicating that they do not have a physical center and that their expansion is regulated by local mechanisms only. The simplest model for a local regulation is that podosomes themselves influence the formation of other podosomes in their immediate surroundings. For example, a podosome could favor podosome assembly on a short range around itself but induce a lasting inhibition at its exact location. The formation of large structures by the interplay of their basic constituents refers to the process of self-organization (Gerhart and Kirschner, 1997), which we propose to control the podosome rings.

The expanding, possibly self-organized ring can therefore explain how podosomes can form the circular patterns found in transformed cells (Gavazzi *et al.*, 1989) and in osteoclasts (Kanehisa *et al.*, 1990; Lakkakorpi and Vaananen, 1991). However, we observed that for several hours during the differentiation process, a majority of the rings, when reaching the cell periphery, disappear. An additional mechanism must promote the stabilization of a ring at the cell periphery to form the podosome belt. Because microtubules have been proposed to regulate podosome formation and distribution (Babb *et al.*, 1997; Linder *et al.*, 2000), we tested whether they could influence podosome dynamics in our system. Strikingly, depolymerization of microtubules by using nocodazole had no effect on podosomes clusters and podosomes rings but had a dramatic destabilization effect on podosome belts. This effect was reversible, indicating that the microtubule network dynamically stabilizes the belt at the periphery of the osteoclast (Figure 7A). It remains to be explained how the regulation by microtubules is modulated during osteoclast differentiation. In conclusion, the combination of two mechanisms, the self-organi-

zation of expanding podosomes rings and the stabilization effect of the microtubule network, allows the formation of the remarkable adhesion apparatus of the osteoclast.

ACKNOWLEDGMENTS

REFERENCES

Akisaka, T., Yoshida, H., Inoue, S., and Shimizu, K. (2001). Organization of cytoskeletal F-actin, G-actin, and gelsolin in the adhesion structures in cultured osteoclast. J. Bone Miner. Res. *16*, 1248–1255.

Arnett, T.R., and Dempster, D.W. (1987). A comparative study of disaggregated chick and rat osteoclasts in vitro: effects of calcitonin and prostaglandins. Endocrinology *120*, 602–608.

Babb, S.G., Matsudaira, P., Sato, M., Correia, I., and Lim, S.S. (1997). Fimbrin in podosomes of monocyte-derived osteoclasts. Cell Motil. Cytoskeleton *37*, 308–325.

Ballestrem, C., Wehrle-Haller, B., and Imhof, B.A. (1998). Actin dynamics in living mammalian cells. J. Cell Sci. *111*, 1649–1658.

Bourette, R.P., Mouchiroud, G., Ouazana, R., Morle, F., Godet, J., and Blanchet, J.P. (1993). Expression of human colony-stimulating factor-1 (CSF-1) receptor in murine pluripotent hematopoietic NFS-60 cells induces long-term proliferation in response to CSF-1 without loss of erythroid differentiation potential. Blood *81*, 2511–2520.

Burgess, T.L., et al. (1999). The ligand for osteoprotegerin (OPGL) directly activates mature osteoclasts. J. Cell Biol. *145*, 527–538.

Chellaiah, M., Kizer, N., Silva, M., Alvarez, U., Kwiatkowski, D., and Hruska, K.A. (2000). Gelsolin deficiency blocks podosome assembly and produces increased bone mass and strength. J. Cell Biol. *148*, 665–678.

Choidas, A., Jungbluth, A., Sechi, A., Murphy, J., Ullrich, A., and Marriott, G. (1998). The suitability and application of a GFP-actin fusion protein for long-term imaging of the organization and dynamics of the cytoskeleton in mammalian cells. Eur. J. Cell Biol. *77*, 81–90.

DeFife, K.M., Jenney, C.R., Colton, E., and Anderson, J.M. (1999). Cytoskeletal and adhesive structural polarizations accompany IL-13-induced human macrophage fusion. J. Histochem. Cytochem. *47*, 65–74.

Gavazzi, I., Nermut, M.V., and Marchisio, P.C. (1989). Ultrastructure and gold-immunolabelling of cell-substratum adhesions (podosomes) in RSV-transformed BHK cells. J. Cell Sci. *94*, 85–99.

Gerhart, J., and Kirschner, M. (1997). Cells, Embryos and Evolution, Malden, MA: Blackwell Science.

Helfrich, M.H., Nesbitt, S.A., Lakkakorpi, P.T., Barnes, M.J., Bodary, S.C., Shankar, G., Mason, W.T., Mendrick, D.L., Vaananen, H.K., and Horton, M.A. (1996). Beta 1 integrins and osteoclast function: involvement in collagen recognition and bone resorption. Bone *19*, 317–328.

Kanehisa, J., Yamanaka, T., Doi, S., Turksen, K., Heersche, J.N., Aubin, J.E., and Takeuchi, H. (1990). A band of F-actin containing podosomes is involved in bone resorption by osteoclasts. Bone *11*, 287–293.

Lakkakorpi, P., Tuukkanen, J., Hentunen, T., Jarvelin, K., and Vaananen, K. (1989). Organization of osteoclast microfilaments during the attachment to bone surface in vitro. J. Bone Miner. Res. *4*, 817–825.

Lakkakorpi, P.T., and Vaananen, H.K. (1991). Kinetics of the osteoclast cytoskeleton during the resorption cycle in vitro. J Bone Miner. Res. *6*, 817–826.

Linder, S., Hufner, K., Wintergerst, U., and Aepfelbacher, M. (2000). Microtubule-dependent formation of podosomal adhesion structures in primary human macrophages. J. Cell Sci. *113*, 4165–4176.

Linder, S., Nelson, D., Weiss, M., and Aepfelbacher, M. (1999). Wiskott-Aldrich syndrome protein regulates podosomes in primary human macrophages. Proc. Natl. Acad. Sci. USA *96*, 9648–9653.

Marchisio, P.C., Bergui, L., Corbascio, G.C., Cremona, O., D'Urso, N., Schena, M., Tesio, L., and Caligaris-Cappio, F. (1988). Vinculin, talin, and integrins are localized at specific adhesion sites of malignant B lymphocytes. Blood 72, 830–833.

Marchisio, P.C., Cirillo, D., Naldini, L., Primavera, M.V., Teti, A., and Zambonin-Zallone, A. (1984). Cell-substratum interaction of cultured avian osteoclasts is mediated by specific adhesion structures. J. Cell Biol. *99*, 1696–1705.

Marchisio, P.C., Cirillo, D., Teti, A., Zambonin-Zallone, A., and Tarone, G. (1987). Rous sarcoma virus-transformed fibroblasts and cells of monocytic origin display a peculiar dot-like organization of cytoskeletal proteins involved in microfilament-membrane interactions. Exp. Cell Res. *169*, 202–214.

Nakamura, I., Pilkington, M.F., Lakkakorpi, P.T., Lipfert, L., Sims, S.M., Dixon, S.J., Rodan, G.A., and Duong, L.T. (1999). Role of $\alpha(v)\beta(3)$ integrin in osteoclast migration and formation of the sealing zone. J. Cell Sci. *112*, 3985–3993.

Nermut, M.V., Eason, P., Hirst, E.M., and Kellie, S. (1991). Cell/substratum adhesions in RSV-transformed rat fibroblasts. Exp. Cell Res. *193*, 382–397.

Ory, S., Munari-Silem, Y., Fort, P., and Jurdic, P. (2000). Rho, and Rac exert antagonistic functions on spreading of macrophage-derived multinucleated cells, and are not required for actin fiber formation. J. Cell Sci. *113*, 1177–1188.

Pfaff, M., and Jurdic, P. (2001). Podosomes in osteoclast-like cells: structural analysis and cooperative roles of paxillin, proline-rich tyrosine kinase 2 (Pyk2) and integrin $\alpha V\beta 3$. J. Cell Sci. *114*, 2775–2786.

Shevde, N.K., Bendixen, A.C., Dienger, K.M., and Pike, J.W. (2000). Estrogens suppress RANK ligand-induced osteoclast differentiation via a stromal cell independent mechanism involving c-Jun repression. Proc. Natl. Acad. Sci. USA *97*, 7829–7834.

Tarone, G., Cirillo, D., Giancotti, F.G., Comoglio, P.M., and Marchisio, P.C. (1985). Rous sarcoma virus-transformed fibroblasts adhere primarily at discrete protrusions of the ventral membrane called podosomes. Exp. Cell Res. *159*, 141–157.

Vaananen, H.K., Zhao, H., Mulari, M., and Halleen, J.M. (2000). The cell biology of osteoclast function. J. Cell Sci. *113*, 377–381.

Wegner, A., Aktories, K., Ditsch, A., Just, I., Schoepper, B., Selve, N., and Wille, M. (1994). Actin-gelsolin interaction. Adv. Exp. Med. Biol. *358*, 97–104.

Zambonin Zallone, A., Teti, A., Gaboli, M., and Marchisio, P.C. (1989). Beta 3 subunit of vitronectin receptor is present in osteoclast adhesion structures and not in other monocyte-macrophage derived cells. Connect Tissue Res. *20*, 143–149.